As originally published in the IPC APEX EXPO Conference Proceedings.

Reliability Study of Low Silver Alloy Solder Pastes

Jennifer Nguyen, David Geiger and Murad Kurwa
Flextronics International
847 Gibraltar Drive
Milpitas, CA, USA

Abstract
Sn3.0Ag0.5Cu (SAC305) is currently the most popular near eutectic lead-free alloy used in the manufacturing processes. Over the last several years, the price of silver has dramatically increased driving a desire for lower silver alloy alternatives.

As a result, there is a significant increase in the number of alternative low/no silver lead-free solder alloys available in the industry recently. Our previous study showed that many alternative low silver solder paste materials had good printing and wetting performance as compared to SAC305 solder pastes. However, there is lack of information on the reliability of alternative alloy solder joints assembled using alternative low silver alloy solder pastes. In this paper, we will present the reliability study of lead-free solder joints reflowed using various lead-free alloy solder pastes after thermal cycling test (3000 cycles, 0°C to 100°C). Six different lead-free pastes were investigated. SAC305 solder joints were used as the control. Low and no silver solder pastes and a low temperature SnBiAg solder pastes were also included.

Keywords: Reliability, lead-free, low Ag alloy, alternative lead free alloy, solder joint reliability, thermal cycling, solder joint microstructure, SnAgCu, SnBiAg, SnCuBi, SnCuNi.

Introduction

Sn3.0Ag0.5Cu solder paste is currently the common alloy for lead-free solder paste in the industry. However, the price of silver has kept increasing over the last several years. This drives the desire for alternative low/no silver alloy materials and leads to the development of many alternative alloys. Today, many alternative low/no silver alloy solder pastes are available in the market. There are publications on the alternative lead-free alloys [1-3]. However, most of the studies focus on the alternative alloys of the BGA solder balls and their reliability. There is very limited publication on the thermal reliability performance of low/no silver alloy solder pastes. In our previous publication [4], alternative low/no silver alloy solder paste performed well in the process evaluation. Many alternative solder pastes had good printability and wettability, as shown in Figure 1 and Figure 2.

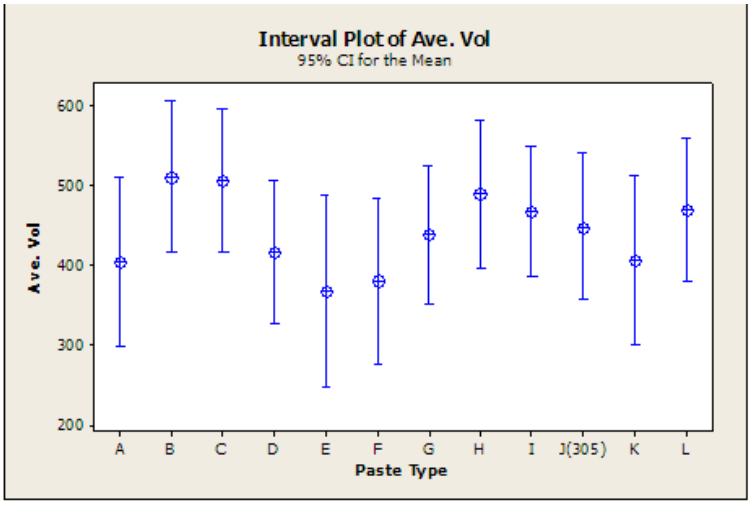

Figure 1 – Printability of low/no silver alloy solder pastes. Paste J was SAC305 solder paste. Other materials were low Ag alloy solder pastes. It showed that many alternative alloy materials had equivalent printing performance as SAC305.

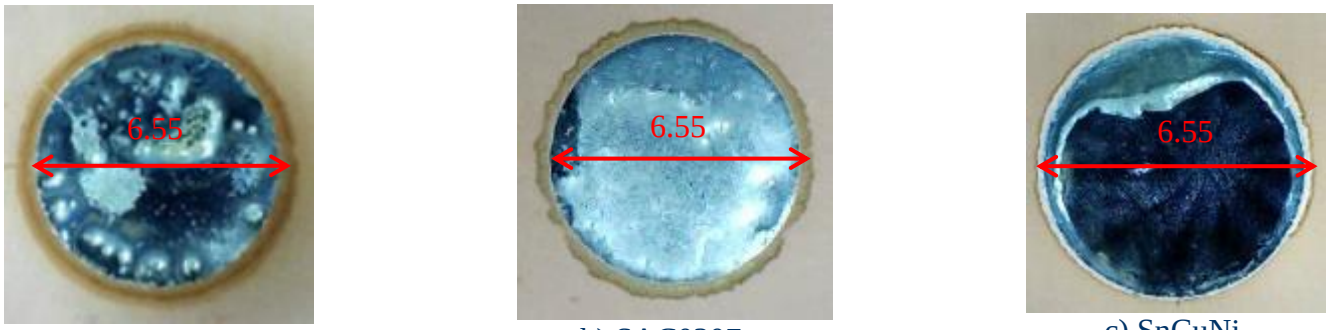

a) SAC305 b) SAC0307 c) SnCuNi

Figure 2 – Wetting Test Results of Various Lead-Free Alloy Solder Pastes. The images of Wetting Test for a SAC305, SAC0307 and SnCuNi alloy solder paste were shown. These three solder pastes had on average a similar spreading diameter.

From the process point of view, the use of alternative alloy solder paste is feasible. However, there is a lack of information on their reliability. In this paper, we will discuss the microstructure, reliability, and failure analysis of lead-free solder joints reflowed using alternative low Ag solder pastes.

Experimental Details

Lead-Free Solder Pastes

Six different lead-free solder pastes were investigated in the study, as shown in Table 1. Type 3 no clean solder pastes were used. Material A, SAC305, was used as the control. Material B, SAC0307, is an alternative low-Ag solder paste without other alloy additions. Material C, SAC0307, contains some micro-alloying additions which can impact the Sn grain coarsening. Material D (SnCuBiCo) and Material E (SnCuNi) have no Ag in their compositions. In addition, a near-eutectic SnBi alloy with a small Ag addition was investigated (Material F). This alloy has a liquidus temperature of around 138°C, which is significantly lower than other tested lead-free alloys. Sn3.0Ag0.5Cu alloy melts at approximately 217 ºC. Alternative low silver high temperature alloys have melting points of around 227-228 ºC. Low temperature Sn-58Bi eutectic is known to be brittle. The small Ag addition is necessary in order to refine the microstructure of the Sn/Bi eutectic, promoting creep deformation by grain boundary sliding over brittle fracture [5]. The alloy compositions of the solder paste materials are listed in Table 1.

Table 1. Solder Paste Materials and their Alloy Compositions.

Item #	Material ID	Alloy Composition	Liquidus Temp. (ºC)
1	Material A	Sn3.0Ag0.5Cu	217
2	Material B	Sn0.3Ag0.7Cu	227
3	Material C	Sn0.3Ag0.7Cu + X (Bi, Sb, etc...)	228
4	Material D	SnCuBi +Co	228
5	Material E	SnCuNi	227
6	Material F	SnBiAg	138

Test Vehicle and Components

The Company Multi-Function Test Vehicle is used in the study (Figure 3). The board dimension is 225mm x 150mm x 1.67mm. The board surface finish is OSP. The test vehicle has many different SMD component types such as BGAs (0.8mm and 1.0 mm pitch), CSP (0.5mm pitch, 0.4mm, 0.3mm), QFN component (0.5mm pitch and 0.4mm pitch), leaded components (SOIC, QFN100, QFN208, etc.), chip components (0201,0402, 0603, 0805), through hole components, etc… In addition, the test vehicle has different areas designed for printability test, slump test, wettability test, solder ball test, pin testability, etc…

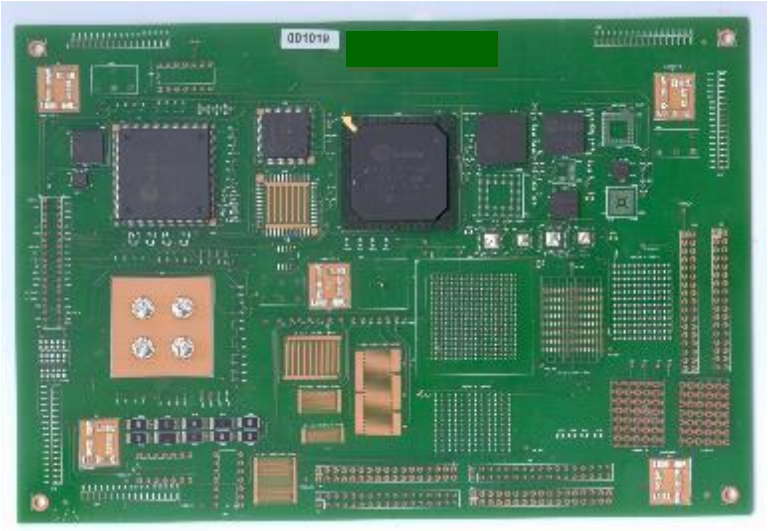

Figure 3 - Company Multi-Function Test Vehicle, Rev 1.0

Components of different types and sizes were assembled for the reliability testing, as shown in Table 3. Daisy chained components were monitored during the thermal cycle test.

Table 2. Components in the Reliability Testing

No	Component Description	Location	Daisy Chain	Board Qty	Alloy Qty	No of Channel
1	A- CABGA196-1.0mm-15mm-DC-LF305	U1	Yes	12	6	72
2	A-CABGA64-.8mm-8mm-DC-LF-305	U300	Yes	12	6	72
3	A-CVBGA97-.4mm-5mm-DC-LF-305	U303	Yes	12	6	72
4	A-CTBGA228-.5mm-12mm-DC-LF-305	U307	Yes	12	6	72
5	A- CABGA1156-1.0mm	U309	Yes	12	6	72
6	Resistors,2512, 0 Ohm	R350-R359	Yes	12	6	72
7	A-QFP208-28mm-.5mm-2.6-DC-Sn	U3	Yes	12	6	72
8	A-MLF32-5mm-.5mm-DC-Sn	U315	No	12	6	N/A
9	A-MLF88-10mm-.4mm-DC Sn	U314	No	12	6	N/A

Assembly Process and Testing Conditions

All the samples using solder pastes A to E were reflowed using a typical lead-free profile with a peak temperature of around 245 °C (Figure 4). SnBiAg paste (material F) was reflowed using a low-temperature reflow profile with a peak temperature of about 170 °C (Figure 5). The reflow was performed in an air atmosphere environment.

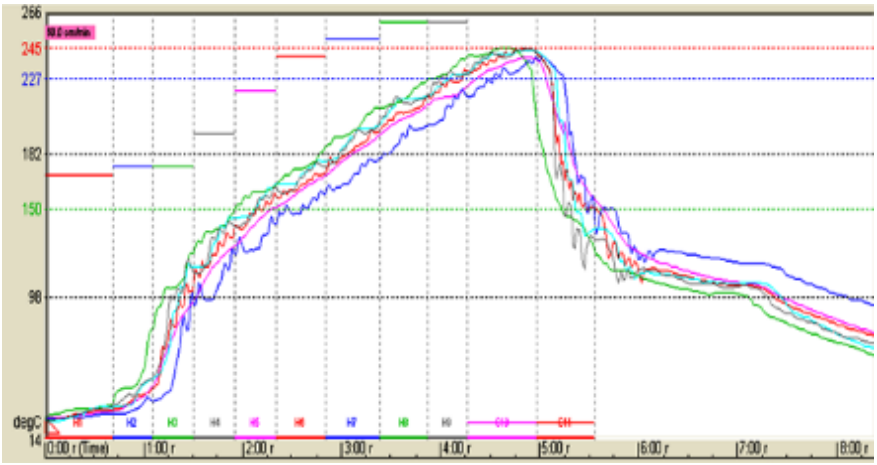

Figure 4. High-temperature Pb-free reflow profile

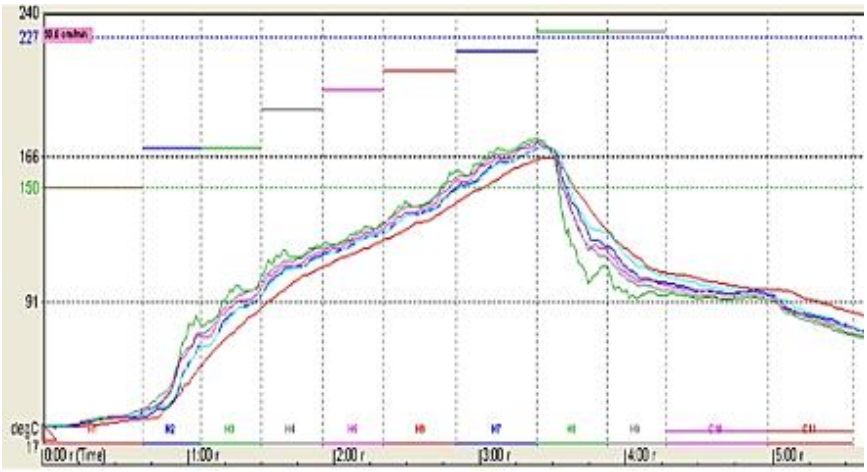

Figure 5. Low-temperature Pb-free reflow profile

The thermal cycle testing was performed in an air-to-air thermal cycle chamber, from 0 to 100 °C with 10-minute dwell time at each peak temperature, and a temperature ramp rate of approximately 10 °C per minute. The chamber profile of temperature versus elapsed time is shown in Figure 6.

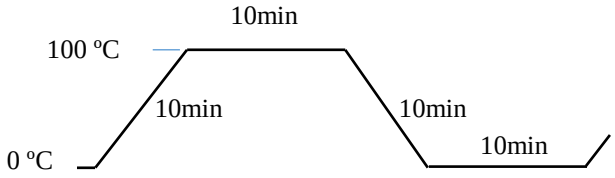

Figure 6. Thermal Cycle Temperature Profile – 0 °C to 100 °C

The thermal cycle test was terminated after 3000 cycles. The resistance of the all components were measured before and after thermal cycle test for failure. Cross sections were performed for the samples before and after the thermal cycle testing.

Results and Discussions

Microstructure Analysis

Intermetallic Layer Thickness

The intermetallic layer thickness was measured for the solder joints assembled with various lead-free alloy solder pastes. The intermetallic layer thickness at the PCB side after the reflow process was between 2 µm to 2.5 µm for SAC 305 material and alternative lead-free high melting temperature alloys. The intermetallic layer thickness at the PCB side after the reflow process for SnBiAg was less than 1 µm. The thin layer formed when using this alloy was due to the low-temperature reflow

profile used. It was noticed that during thermal cycle testing the IMC layer of SnBiAg grew significantly to around 2µm, which was similar to the intermetallic layer thickness of other tested lead-free alloys. There was no significant change in the IMC thickness for SAC 305 and alternative low/no silver high temperature alloys after thermal cycle testing. The thicknesses of the intermetallic layer at the PCB side after reflow and after the thermal cycle test were shown in Figure 7.

The intermetallic layer thickness at the component side after the reflow process was around 1.5 µm to 2 µm. It was slightly thinner than the IMC thickness at the PCB side. Similarly, the IMC thickness at the component side for alternative low silver high temperature alloys after thermal cycle testing was not changed significantly. The IMC thickness of low temperature SnBiAg was thin (~1.2 µm) after the reflow process. This thickness increased to around 1.7 µm after the thermal cycle testing. The thickness of the intermetallic layer at the component side was shown in Figure 8.

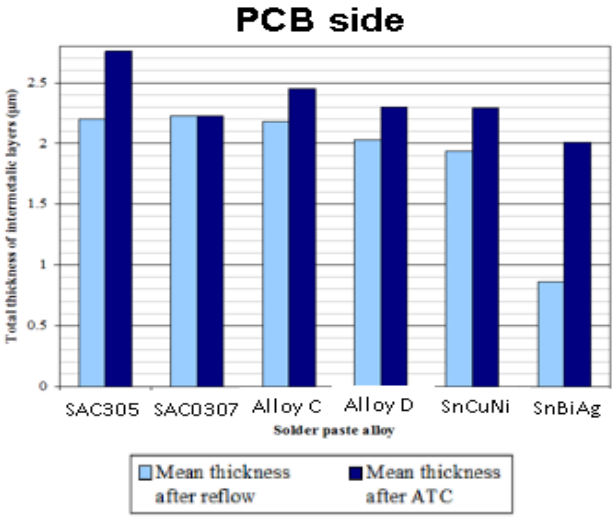

Figure 7. Intermetallic layer thickness measurements at the PCB side after reflow and after thermal cycle testing.

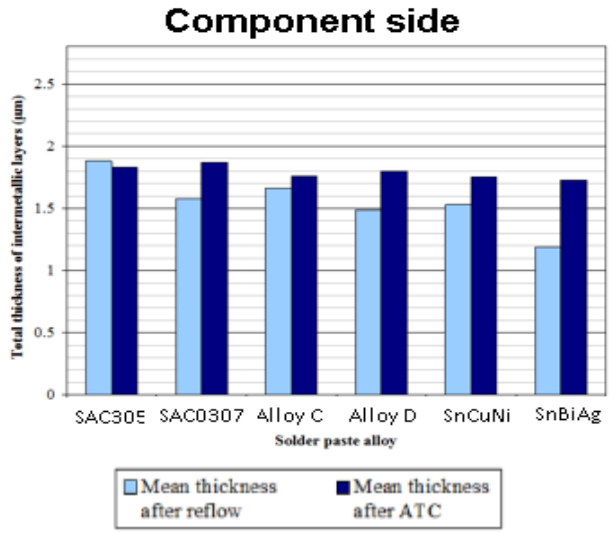

Figure 8. Intermetallic layer thickness at component interface after reflow and after thermal testing.

Microstructure Analysis after Reflow Process

The cross-sections of all components were performed after the reflow process. In general, good solder joints were observed for alternative alloys. Incomplete mixing was seen for the most BGA components reflowed with the SnBiAg solder paste. The inhomogeneous solder joint was observed due to the low temperature profile used for SnBiAg solder paste. Head in pillow (HiP) solder joint was also seen for the large components such as BGA1156 reflowed with SnBiAg solder paste. The cross section images of BGA solder joint reflowed using alternative alloy solder pastes are shown in Figure 9.

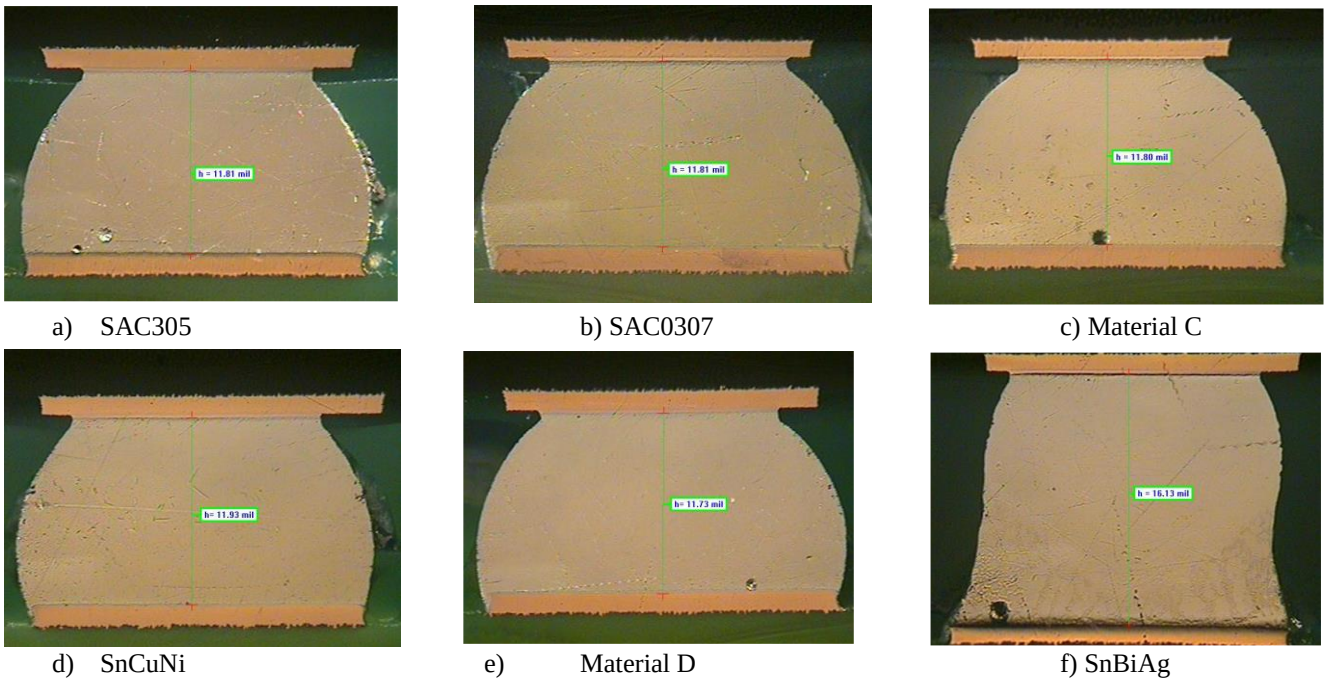

a) SAC305 b) SAC0307 c) Material C

d) SnCuNi e) Material D f) SnBiAg

Figure 9. Cross Section Images of BGA 196 components after Reflow Process

The solder joint microstructure of the alloys were further analysed using a scanning electronic microscope (SEM). Cu_6Sn_5 intermetallic layer was the common feature for all alloy solder joints. For SAC305 solder joint, Sn IMC were mostly seen in the solder joint, along with Ag_3Sn and Cu_6Sn_5 intermetallic species (Figure 10a). Areas of both the Sn/Ag_3Sn binary eutectic and the $Sn/Ag_3Sn/Cu_6Sn_5$ ternary eutectic were visible at grain boundaries of the Sn dendrites. The presence of the Sn/Ag_3Sn binary eutectic suggesting that Cu_6Sn_5 was the last phase to solidify. In samples reflow with SAC0307 solder paste, the reduction in Ag content of SAC0307 solder paste resulted in a reduction in the number of Ag_3Sn particles in the solder joint microstructure, accompanied by the formation of larger Sn dendrites (Figure 10b). Large areas of Ag_3Sn/Sn binary eutectic were not visible. The microstructure of Material C solder joint after reflow showed that Cu_6Sn_5 particles in the bulk of the solder appeared smaller in Material C than in SAC0307 (Figure 10c). However, compared to SAC0307, the doped alloy did not show any statistically significant difference in the composition or thickness of the intermetallic layers. The BGA solder joints of both alloys were also similar, closely resembling those of the all-SAC305 assembly, though in both cases there was a slight reduction in the size of the Ag_3Sn particles.

The microstructure of SnCuNi and Material D solder joints are shown in Figure 10d and Figure 10e, respectively. Both alloys contained no silver in the solder paste. Cu_6Sn_5 intermetallic layer was seen in the solder joint. Material D solder joints displayed an even distribution of Cu_6Sn_5 particles, and the grain size of the Sn dendrites was small compared to the other high-temperature alloys. The Cu_6Sn_5 grains were typically larger than in SnCuNi, which is an Ag-free alloy with a higher concentration of Cu than Material D. This implies that Cu_6Sn_5 formed as the primary phase with less undercooling than would be expected.

In the SnBiAg solder joint microstructure, the majority of the solder joint consisted Bi and Sn dendrites (Figure 10f). Small grains of Ag_3Sn were visible at grain boundaries, as were Cu_6Sn_5 particles near the solder pads. It was noticed that Bi dendrite boundary was not well defined after the reflow process.

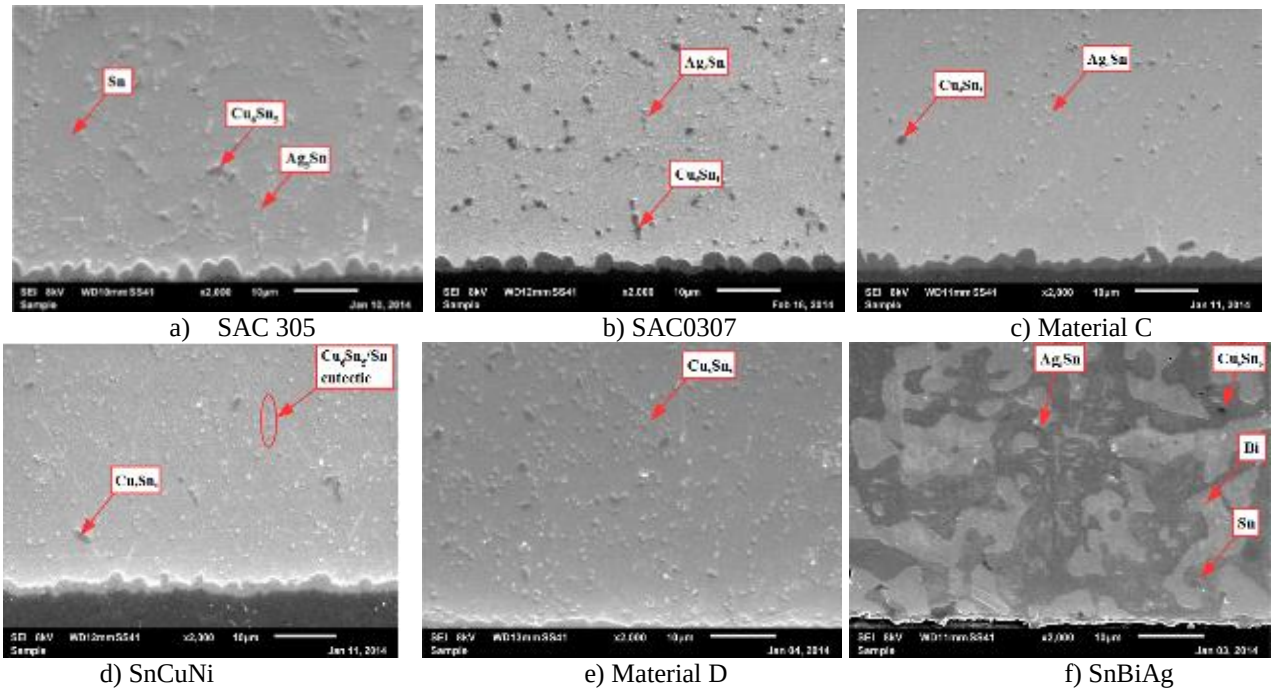

a) SAC 305 b) SAC0307 c) Material C

d) SnCuNi e) Material D f) SnBiAg

Figure 10. SEM Images of QFN solder joint reflowed with various alloy solder pastes. a) SAC305; b) SAC0307; c) Material C; d) SnCuNi; e)Material D; f) SnBiAg

Thermal Cycle Test Results

Results after 3000 Cycles

Table 3 summarizes the thermal cycle test results of different components reflowed using different lead-free alloy solder pastes. In general, SAC305 had a better thermal reliability than alternative low Ag alloy materials. The thermal reliability performance depended on the component types and the component design/material. Complete failure was observed for some BGA 196 components, BGA228 components, BGA97 components and resistor 2512 components after 3000 cycles (0°C to 100°C). Major cracks were seen at their solder joint. The cross section images of BGA196 solder joint after thermal cycling test are shown in Figure 11. Most cracks happened at the component side of the package although some cracks were also observed at the PCB side. Solder joint reflowed with SnBiAg also had cracks at the interface of SAC305 solder ball and SnBiAg solder paste. The cross sections of 2512 resistors and QFN88 components after thermal cycle test were shown in Figure 12 and Figure 13, respectively. Severe cracking in the solder joint were seen for these components.

Table 3. Thermal Cycle Test Results

Thermal Cycling Test Summary	Number of Failed Components After 3000 Cycles							
	U309 (BGA1156)	U1 (BGA196)	U307 (BGA228)	U303 (BGA97)	U300 (BGA64)	U3 (QFP204)	U20 (QFP144)	R2512
SAC305	0/12	0/12	3/12	0/12	0/12	0/12	0/12	2/12
SAC0307	0/12	3/12	5/12	0/12	0/12	0/12	0/12	12/12
Alloy C	0/12	4/12	6/12	0/12	0/12	0/12	0/12	11/12
Alloy D	0/12	4/12	6/12	1/12	0/12	0/12	0/12	12/12
SnCuNi	0/12	2/12	5/12	1/12	0/12	0/12	0/12	12/12
SnBiAg	12*/12	5/12	7/12	1/12	1/12	0/12	0/12	2/12

a) SAC305 b) SAC0307 c) Material C

d) SnCuNi e) Material D f) SnBiAg

Figure 11. Cross section images of BGA196 components after 3000 thermal cycles. a) SAC305; b) SAC0307;c) Material C; d) SnCuNi; e) Material D; f) SnBiAg.

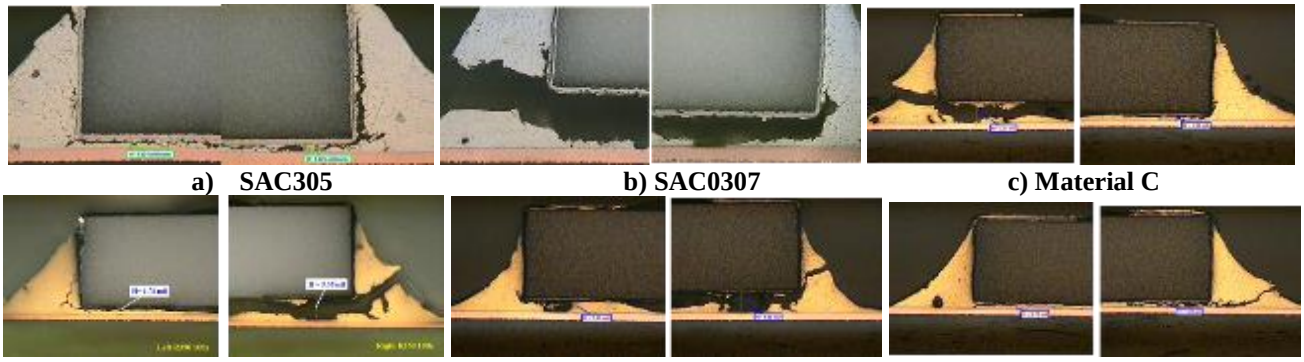

a) SAC305 b) SAC0307 c) Material C

d) SnCuNi e) Material D f) SnBiAg

Figure 12. Cross section images of R2512 solder joint assembled using different Pb-free alloy solder pastes after 3000 thermal cycles a) SAC305; b) SAC0307; c) Material C; d) SnCuNi; e)Material D; f) SnBiAg

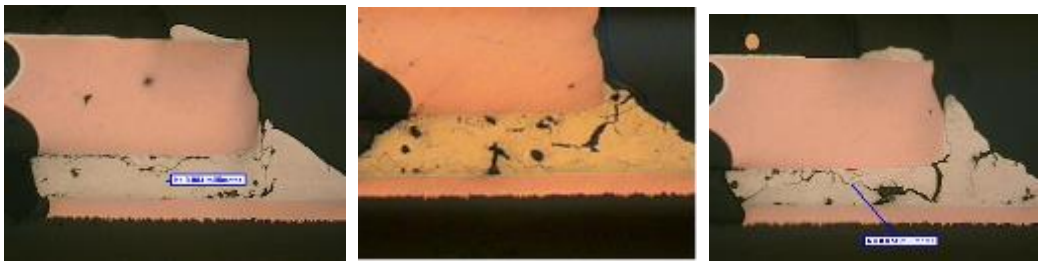

a) SAC305 b) SAC0307 c) Material C

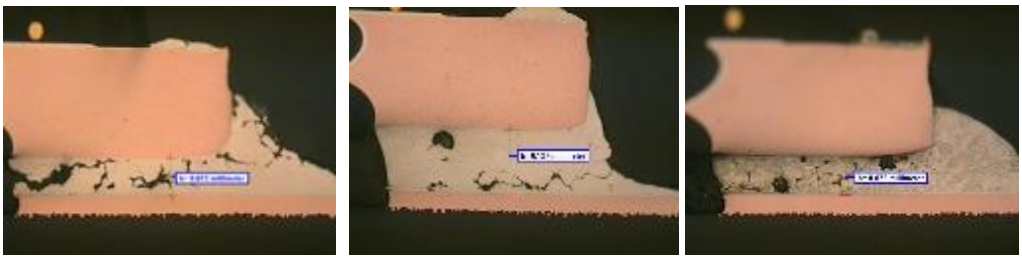

d) SnCuNi **e) Material D** **f) SnBiAg**

Figure 13. Cross section images of QFN solder joint assembled using different Pb-free alloy solder pastes after thermal cycle testing. a) SAC305; b) SAC0307; c) Material C; d) SnCuNi; e) Material D; f) SnBiAg

No failure was observed for some BGA components such as BGA1156 (1.0mm pitch, 35mmx35mm) and BGA64 component (0.8mm pitch, 8mm X 8mm) after thermal cycle testing. Only minor cracks were seen. The cross sections of BGA1156 component are shown in Figure 14. Minor cracking and no failure was also observed for QFP components in this study (Figure 15).

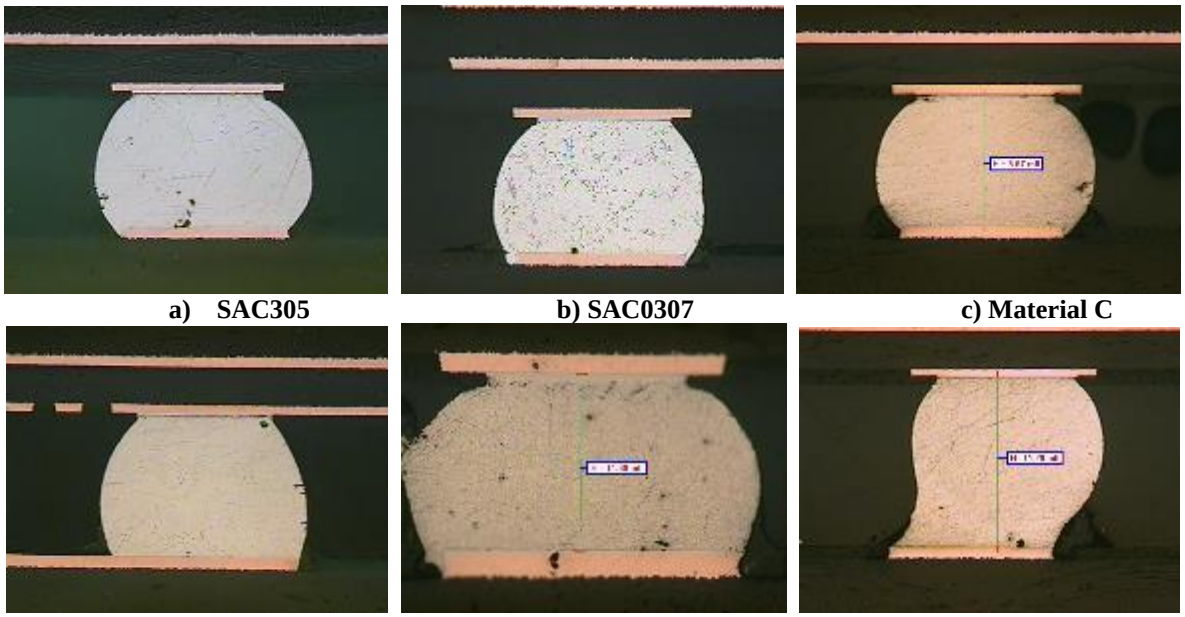

a) SAC305 **b) SAC0307** **c) Material C**

d) SnCuNi **e) Material D** **f) SnBiAg**

Figure 14. Cross section images of BGA1156 solder joint after thermal cycle testing. a) SAC305; b) SAC0307; c) Material C; d) SnCuNi; e) Material D; f) SnBiAg

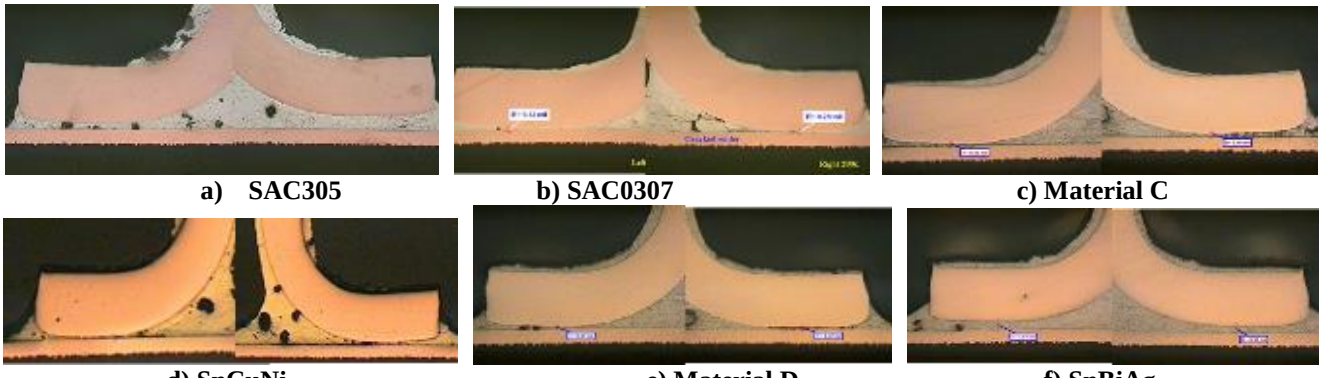

a) SAC305 **b) SAC0307** **c) Material C**

d) SnCuNi **e) Material D** **f) SnBiAg**

Figure 15. Cross section images of QFP208 solder joint assembled using different Pb-free alloy solder pastes after thermal cycle testing. a) SAC305; b) SAC0307; c) Material C; d) SnCuNi; e) Material D; f) SnBiAg

Microstructure Analysis after Thermal Cycle Test

Microstructure of various alloys after thermal cycle testing was analysed with SEM equipment. Within SAC305 solder joints, blocky Cu_6Sn_5 particles formed and Ag_3Sn particles had begun to elongate (Figure 16). Some inter-granular cracking was visible at the boundaries between Sn dendrites as well as between dendrites and intermetallic species. Cracking along the intermetallic layers was also observed.

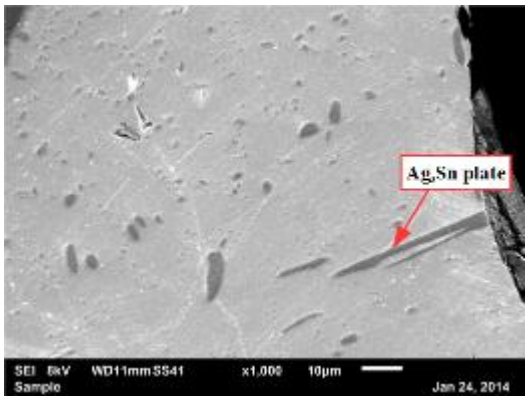

Figure 16. Ag_3Sn plate formation in QFP solder joint assembled using SAC305 paste after thermal cycle testing.

Using SAC0307 solder, the number and size of the Ag_3Sn grains was reduced. Unlike SAC305, thermal cycling did not result in the formation of large Ag_3Sn plates (Figure 17). However, dislocations along grain boundaries were visible, and more extensive than for SAC305, indicating that the coarsening of Sn dendrites does increase their tendency to crack.

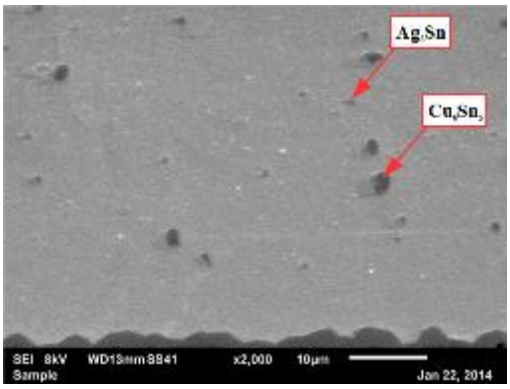

Figure 17. Microstructure of QFN88 solder joint assembled using SAC0307 paste after thermal cycle testing.

Material C behaved in a similar fashion to SAC0307, showing extensive cracking along grain boundaries in almost all samples. The BGA solder joints showed a reduction in the growth rate of Ag_3Sn particles compared to SAC0307. In the lower half of the Material C BGA solder joints, larger particles of Cu_6Sn_5 were observed (Figure 18).

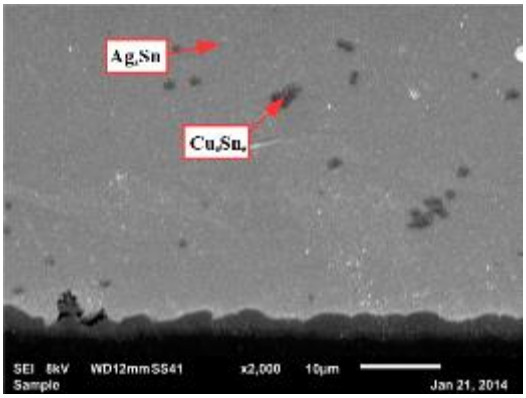

Figure 18. Microstructure of QFN88 solder joint assembled using Material C solder paste after thermal cycle test.

The layer of Cu_3Sn adjacent to the PCB pad was thinnest for solder joints composed of SnCuNi solder, suggesting that the insertion of Ni into the intermetallic layers reduced the rate of diffusion within the crystal structure (Figure 19).

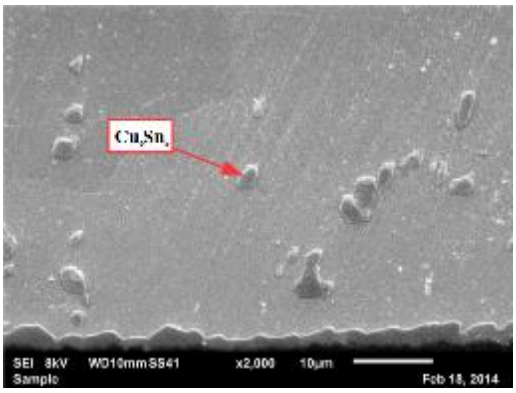

Figure 19. Microstructure of QFN88 solder joint assembled using SnCuNi solder paste after thermal cycle test.

Relatively little coarsening of the microstructure of Material D solder joints occurred after thermal cycle testing. Sn dendrites and Cu_6Sn_5 were visible (Figure 20). There are several possible explanations for how little coarsening was observed. Firstly, Co has previously been shown to substitute for Cu in Cu_6Sn_5 grains, introducing a substitutional defect which inhibits coarsening [6]. The presence of a low concentration of Bi is known to have a Zener pinning effect on Sn grains, which increases the energy barrier to grain growth [7]. Cracking of the BGAs largely occurred at the bottom of the solder joint, as opposed to at the top. Under strain, the more brittle solution-hardened Sn matrix formed by Material D was more likely to crack than the more ductile Sn matrix at the top of the solder joint, which had a composition close to that of SAC305.

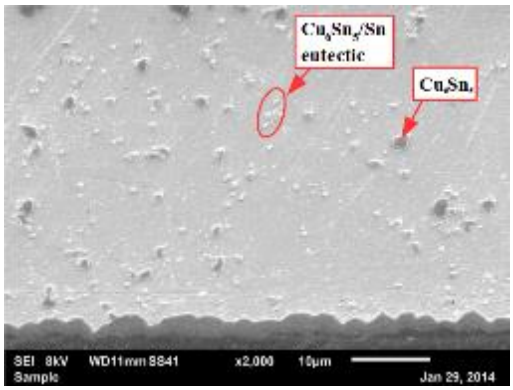

Figure 20. Microstructure of QFN88 solder joint assembled using Material D solder paste after thermal cycle test.

Figure 21 shows the typical microstructure of SnBiAg after thermal cycling. By far the most growth in the intermetallic layers occurred in the SnBiAg solder joints, some of which were more than doubled in thickness during thermal cycle testing. The thickness of the intermetallic layers became comparable to those formed by the other solder alloys, suggesting that the thin layers observed prior to thermal cycle test were at least in part a result of the low reflow temperature. The concentration of Sn in the solder appeared to have little effect on the intermetallic layer thickness. A Cu_3Sn layer formed, similar to in thickness to that of the SnAgCu alloys. Coarsening of the Sn and Bi dendrites occurred. Both Ag_3Sn and Cu_6Sn_5 particles increased in size. Cu_6Sn_5 particles, found close to the Cu solder pads, were also more frequent, indicating further dissolution of Cu from the solder pads into the bulk of the solder occurred during thermal cycle testing.

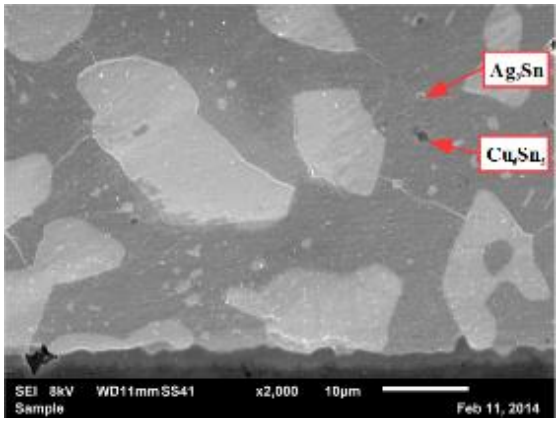

Figure 21. Microstructure of QFN88 solder joint assembled using SnBiAg solder paste after thermal cycling.

Failure Mode Analysis

For the single-alloy QFP and QFN components, four different typical failure modes were observed. For SAC305 solder joints, cracking was primarily propagated along Cu_6Sn_5 and Ag_3Sn intermetallic particles in the bulk of the solder (Figure 22). The single-alloy solder joints assembled with SAC0307, Material C and SnCuNi, in which far fewer intermetallic species were present, all showed evidence of ductile fracture at the grain boundaries between Sn dendrites, as shown in Figure 23. This was typically more severe than the cracking observed using SAC305 in the same components. Material D displayed a lesser degree of cracking than these three alloys. Cracking appeared to propagate at Sn grain boundaries (Figure 24). The SnBiAg solder joints displayed a different failure mode. Cracks were formed primarily as a result of grain boundary sliding (Figure 25). Some cracking through Sn grains also occurred as a result of the embrittlement caused by dissolution of bismuth in the tin matrix.

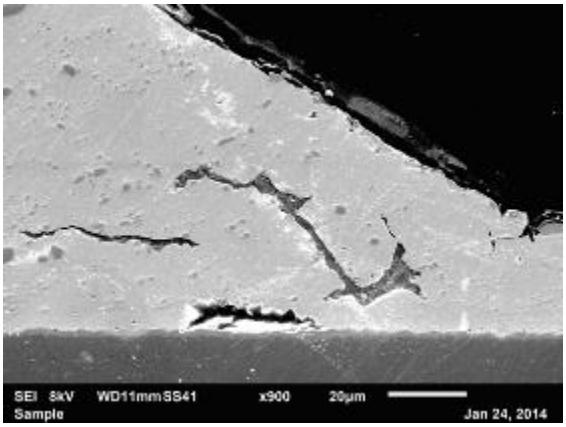

Figure 22. Typical cracking in QFP208 solder joint assembled using SAC305: ductile fracture propagating along grain boundaries of intermetallic species

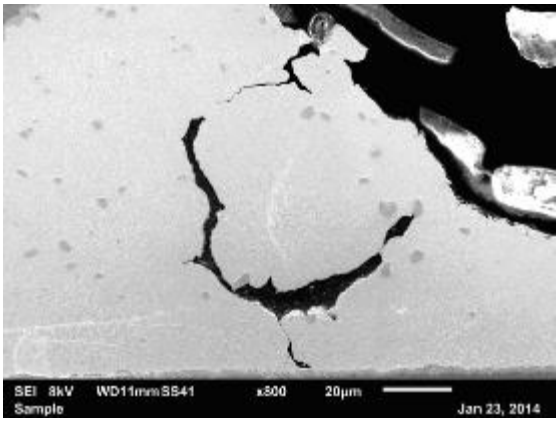

Figure 23. Cracking along Sn grain boundaries in QFP208 solder joint assembled using SAC0307

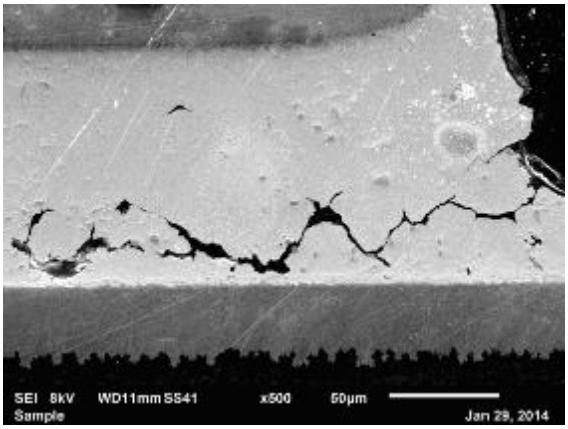

Figure 24. Cracking along Sn grain boundaries in QFN88 solder joint assembled using Material D

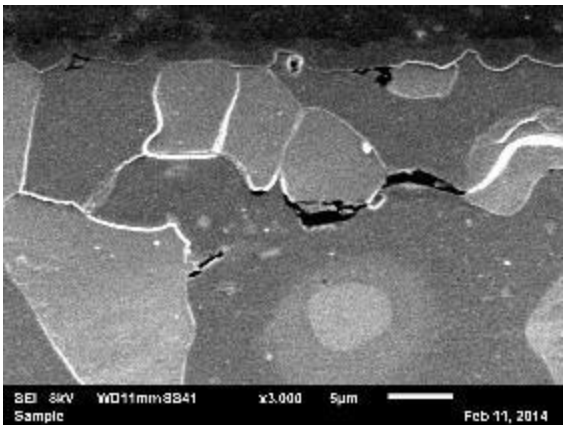

Figure 25. Cracking in QFN88 solder joint assembled using SnBiAg solder paste.

In the BGA solder joints, different effects were observed as a result of the mixing of the alloys. Cracking propagating along the grain boundaries of intermetallic species within the bulk of the solder joint were observed for the majority of components. However, the severity of this cracking was dependent on the solder paste alloy. More cracking appeared to occur when any of the four high-temperature low-silver alloys were used.

An increase in ductile fracture at the bottom of the solder joint is observed when using Material D solder. It is expected that as this alloy forms a more brittle solder joint than the others, a result of the Bi addition, that the upper part of the solder joint, in which SAC305 predominates, is more prone to plastic deformation than the lower part, which is likely to have a higher Bi content.

Many BGA solder joints assembled with SnBiAg solder paste remained inhomogeneous after thermal cycle test. Creep deformation of the BGA solder joints was visible. Grain boundary sliding occurred at the bottom of the solder ball, in the region composed primarily of Sn and Bi dendrites. It was observed that the SnBiAg solder joints cracked less than the low Ag high-temperature alloys for some of the BGA components and more for others. Cracking within the SAC305 area was less common than cracking within the SnBiAg area, the latter being more susceptible to deformation under strain. In several cases, cracking was visible at the interface between the SnBiAg and the SnAgCu regions of the BGA

Conclusions

There is no significant difference in the intermetallic layer thickness of the solder joints assembled with SAC305 and other alternative high temperature low-Ag, Pb-free alloy solder pastes (SAC0307, SnCuNi, Material C,Material D). In general, the IMC thickness of these materials slightly increased after thermal cycle test, but the change was negligible. The IMC thickness of the SnBiAg solder joints after reflow process was typically thinner than those of the high temperature lead-free alloys. The IMC layer of SnBiAg solder joints grew during the thermal cycle testing, to a similar IMC thickness to the other lead-free alloys. The thickness and composition of the intermetallic layers was not determined to affect the reliability of the solder joint during the thermal cycle testing.

The thermal reliability of alternative lead-free solder joint varied depending on the package types and the component size. In our study, this factor affected the solder joint's thermal reliability more than the impact of alloy composition of the solder paste. The 2512 resistors was failed first as compared to other tested components. Complete failure and sever cracking were seen for most 2512 resistors after 3000 thermal cycles (0°C to 100°C). No complete failure was observed for small chip component such as 0603, 0402, 0201 components after the testing. Severe cracking and some failure were also observed for BGA196, BGA228, BGA97 and QFN88 after the thermal cycle testing. Minor cracking and no failure was seen for BGA1156, BGA64, QFN32, and QFP208 and QFP100 components. In general, solder joint assembled with SAC305 solder pastes still performed better than low Ag alloy solder pastes. Unexpectedly, low temperature SnBiAg solder joint performed well after thermal cycle test when it was the single alloy in the solder joint. When SAC 305 BGA reflowed with SnBiAg solder pastes, more defects and failures were seen. Further reliability study should be done for alternative lead-free alloy solder paste materials.

Acknowledgements

The authors would like to thanks Elissa McKay and Tu Tran at the company AEG labs for their help in the cross sections and failure analysis of this study.

References

1. J. Smetana, R. Coyle, P. Read, T. Koshmeider, D. Love, M. Kolenik and J. Nguyen, " Thermal Cycling Reliability Screening of Multiple Pb-Free Solder Ball Alloys," *Proceeding of APEX conference*, 2010.
2. G. Henshall, et al., "INEMI Pb-Free Alloy Characterization Project Report: Part I-Program Goals, Experimental Structure, Alloy Characterization and Test Protocols for Accelerated Thermal Cycling," *Proceeding of SMTAi*, 2012.
3. K. Sweatman, et al., "iNEMI Pb-Free Alloy Characterization Project Report: Part III – Thermal Fatigue Results for Low Ag Alloys" *Proceeding of SMTAi*, 2012.
4. Jennifer Nguyen, et al., "Assembly Process Feasibility of Low/No Silver Alloy Solder Paste Materials" *Proceeding of APEX conference*, San Diego, 2013.
5. S. Sakuyama, T. Akamatsu, K. Uenishi, T. Sato, Trans. Japan Inst. Electron. Packaging V.2, 2009, pp. 98-103.
6. I. E. Anderson, B. A. Cook, J. L. Harringa, R. L. Terpstra, J. Electron. Mater. V.31, 2002, pp. 1166-1174.
7. H. Shimokawa, T. Soga, K. Serizawa, Mater. Trans. V.8, 2002, pp. 1808-1815.